

---

## ***Supplementary Material:***

# **Pond dynamics and supraglacial-englacial connectivity on debris-covered Lirung Glacier, Nepal**

**Evan S. Miles**<sup>1,2\*</sup>, **Jakob Steiner**<sup>3,4</sup>, **Ian Willis**<sup>1</sup>, **Pascal Buri**<sup>4</sup>, **Walter W.**

**Immerzeel**<sup>3</sup> **Anna Chesnokova**<sup>4,5</sup> and **Francesca Pellicciotti**<sup>4,6</sup>

<sup>1</sup>*Scott Polar Research Institute, University of Cambridge, Cambridge, UK*

<sup>2</sup>*School of Geography, University of Leeds, Leeds, UK* <sup>3</sup>*Department of Geography, University of Utrecht, Utrecht, Netherlands*

<sup>4</sup>*Institute of Environmental Engineering (IfU), ETH-Zürich, Zürich, Switzerland*

<sup>5</sup>*Département de génie de la construction, École de technologie supérieure, Montreal, Quebec*

<sup>6</sup>*Department of Geography, University of Northumbria, Newcastle-upon-Tyne, UK*

Correspondence\*:

E.S. Miles

e.s.miles@leeds.ac.uk

## **1 INTERPRETATION OF WATER LEVEL RECORDS**

Changes in pond water level could be the expression of a variety of disturbances, including a large debris slump (whether a single large boulder or many small clasts), small but frequent debris slumps, calving and similar structural collapse sourced above the water level, floor collapse beneath the water level, subaqueous melt, and variations in the balance between water inputs from upstream melt and rainfall, and outflow discharge. As we do not have direct evidence to distinguish between these processes during the monsoon, we characterise the rate and magnitude of water level change resulting from each potential source to attribute measured water level changes to different sources.

- **Positive displacements:** A large debris slump, such as a boulder falling into the pond, would be likely to create a sharp rise. If there is an outlet for the pond, this would be followed by a decay of the displaced hydraulic head. Calving and other structural collapses sourced from above the pond's water level would have a similar effect, by displacing a large volume of the pond, causing a sharp increase in hydrostatic head. For small ponds, even small volumetric inputs would produce a measurable increase

in head. For larger ponds, only extremely large volumetric inputs would cause an identifiable head increase. Smaller debris slumps, as observed regularly for ponds bordered by ice cliffs, would also cause a momentary displacement. However, they are likely to be too small to be identified in the signal, and their relatively high frequency means that they would simply contribute to signal noise.

- Negative displacements: A collapse of the pond's floor (e.g. as identified in the Mertes et al., 2016, conceptual model) is effectively a sudden basin expansion, and would result in a lowering of the pond's water level. The pressure transducer's position will determine how this event is recorded. If the collapse occurred directly beneath the sensor, the sensor would likely lower more than the water level, and a sharp increase in pressure would be observed. If the collapse was elsewhere in the pond floor, the water level would drop above the sensor, and a drop in pressure would be measured. However, as with a positive displacement, the volume of the collapse would have to be sufficiently large to be identifiable in the pressure record. Unless the collapse changed the pond's outlet structure, the water level would rise to its previous level (or above if there was no outlet).
- Basin expansion: Subaqueous melt would lead to a lowering of the water level as the basin expanded due to the density difference between water and ice. The melt rate might be expected to vary diurnally and seasonally due to the pond's surface energy balance and the rate of overturning, leading to a pulse of basin expansion below the waterline (Miles et al., 2016).
- Local catchment ablation: Variations in local meltwater supply would lead directly to changes in pond water level. Such variations would have a diurnal structure (Benn et al., 2017; Horodyskyj, 2017) due to varying temperatures, but may lag air temperatures due to delay by overland flow through the surface debris. Meltwater supply also varies seasonally (e.g. Ragetti et al., 2015), and this would lead to changes in the magnitude of diurnal variations recorded. However, such diurnal variations may be reduced for larger ponds compared to smaller ponds. Importantly, variations in water supply would only generate an increase in water level (a staircase signal) unless the pond has an outlet.
- Precipitation: Large precipitation events would be evident as a progressive water level rise, as overland flow through the debris would delay delivery to the pond. If the pond has an outlet, pond flooding would be followed by drainage, leading to a pulse-like signal.
- Distal sources: Water supply from distal sources would give a signal similar to that of precipitation (e.g. a pulse or progressive rise) or local melt (diurnal variations) but with a magnitude and timing inexplicable by those mechanisms.
- Drainage: Significant pond drainage would lead to pronounced water level decline. Glaciospeleological observations indicate that primary englacial drainage mechanisms should lead to rapid drainage for perched ponds (Gulley et al., 2009; Benn et al., 2012). These include hydrofracturing (which would

lead to sudden drainage), and connection with relict englacial conduits (which could also lead to sudden drainage). Conversely, drainage via a spillway (whether englacial or superficial), on the other hand, would be manifested as a relatively slow water level lowering. Seepage through a frozen debris matrix might also be expected to produce slow drainage. However, Gulley et al. (2009) noted that flow through debris-filled crevasse traces or fractures will develop into a conduit as pore space enlarges.

Based on these characterisations, we interpret each water level record. As an example, here we interpret the variety of short-term changes at pond D in 2014 (Figure 4). Small debris slumps are not identifiable, and we cannot distinguish between different types of positive displacements (calving vs debris). However, positive displacements are followed by a decay on several occasions (e.g. 5 July, 6 July, 16 July, 20 July, and 28 July, magnitudes of 0.08–0.20 m), and suggest that the pond has an outlet of some sort during these times. There are three instances of sharp water level rises not followed by decay (12 June, 13 June, 2 July; magnitudes of 0.09–0.16 m), which likely corresponds to floor collapse beneath the sensor or sudden distal changes in water supply. An even larger, sharper increase (0.45 m) without subsequent decay occurs on 2 August. There are three sharp drops of water level (2 on 29 June, 3 July; magnitudes of 0.07–0.18 m) which likely correspond to basin expansion away from the sensor.

## 2 DETERMINATION OF POND WATER SOURCES

We perform back-of-the-envelope calculations to assess the plausibility of different possible causes of water level rise (Table S1). In particular, we assess the volumes of water associated with four seasonal pond-filling events (ponds C and D in 2014, and pond J in both 2013 and 2014; Figures 3 and 4), as well as for several shorter-duration variations captured by the water level logs at ponds C and D in 2014. For each event, the net (difference between start and finish) and cumulative (summing all rises) water level rise is measured from the hourly water level record. The pond's mean area over the filling period is estimated based on the orthoimage closest in time, accounting for water level change in the intervening period. This enables us to estimate the volume added to the pond over the filling period.

To calculate potential water supplies from the pond's local surface catchment, we first determine the catchment area based on our surface drainage analysis of the SPOT6 DEM. We then use the on-glacier 2m air temperature logger (Table 1) to calculate the positive degree-days (PDD) over the period of water level rise. (Immerzeel et al., 2014b) determined a mean degree-day factor of  $0.74 \text{ mm } ^\circ\text{C}^{-1} \text{ d}^{-1}$  for Lirung Glacier in 2013, and we use this value to calculate the mean ablation over the period of water level rise. We also determine cumulative precipitation over the period from the Kyanjing AWS (Table 1). Finally, the calculated ablation and measured precipitation are multiplied by the pond's catchment area to estimate local inputs.

## 2.1 Seasonal filling events

We first assess whether local water supplies (ablation and precipitation) can account for the select long-term water level rises:

- *Pond C, 2014*: The major water level rise observed at pond C in 2014 occurred between 15 March and 21 April, a period of 37 days (Figure 4). Nearby sensors recorded only 59.6 PDD over this period, and 41.4 mm of precipitation. Given the pond's catchment area of 39,100 m<sup>2</sup>, local catchment inputs of meltwater and precipitation were estimated at 1619 m<sup>3</sup> and 1725 m<sup>3</sup>, respectively, for a total of 3343 m<sup>3</sup>. The pond experienced a net water level increase of 1.85 m, but a cumulative total of 2.21 m including all diurnal rises. We estimate an average area of 600 m<sup>2</sup> for the pond based on the observed areas in April and May. This corresponds to a net increase in pond volume of 1110 m<sup>3</sup> during the water level rise, or a cumulative increase of 1326 m<sup>3</sup>. This is less than the local inputs due to early premonsoon melt and precipitation, indicating that local water supply could be the cause for the pond flooding.
- *Pond D, 2014*: A gentle rise of water level was observed at pond D between 6 May and 18 June (43 days, Figure 4). 77.9 mm of precipitation was observed over this period, and the late pre-monsoon conditions led to a total of 321.9 positive degree days. The pond's catchment area was 19,400 m<sup>2</sup>, so for total water supply from precipitation we calculate 1511 m<sup>3</sup> and from melt we estimate 4621 m<sup>3</sup>, for a total of 6132 m<sup>3</sup>. Water level rose a net 1.1 m over this period, and we estimate a mean pond area of ~ 400 m<sup>2</sup>, leading to a net storage increase of only 440 m<sup>3</sup>. Accounting for diurnal rises, a cumulative increase of 2.7 m was registered, representing a total volume increase of 1060 m<sup>3</sup> over the period. For this water level rise, supply from the local catchment is more than the overall change in volume and also accounts for the daily variations in water level.
- *Pond J, 2013*: In 2013, the pressure transducer at pond J recorded a net rise of 1.22 m between 11 May and 11 June (31 days, Figure 3). This period corresponded to 76.6 mm precipitation and 237.1 PDD. With a catchment area of 83,800 m<sup>2</sup>, the pond would have been locally supplied by 6419 m<sup>3</sup> from precipitation and 14,703 m<sup>3</sup> from meltwater, for a total local supply of 21,122 m<sup>3</sup>. The pond's area was at least 7300 m<sup>2</sup> over this period, indicating a net volume change of 8906 m<sup>3</sup> or more. Accounting for diurnal rises, a cumulative increase of 1.8 m was registered, representing a total input of 13,067 m<sup>3</sup> over the period. As at ponds C and D, supply from the local catchment is enough to explain the overall change in volume as well as the daily variations in water level.
- *Pond J, 2014*: The pressure transducer at pond J recorded a net rise of 6.2 m between 21 April and 7 June (47 days, Figure 4). Nearby sensors observed 87.5 mm precipitation and 274.2 PDD during this period. Again using a catchment area of 83,800 m<sup>2</sup>, the pond would have been locally supplied by

7333 m<sup>3</sup> from precipitation and 17,004 m<sup>3</sup> from meltwater, for a total local supply of 24,337 m<sup>3</sup>. The pond occupied at least 4000 m<sup>2</sup> during this period, as the SPOT6 orthoimage corresponds to the lowest water level. By flooding the SPOT6 DEM to various levels, we estimate a mean area of 6000 m<sup>2</sup> over this period for a net volume change of 37,800 m<sup>3</sup>. Diurnal rises add very little to the cumulative water level increases (6.3 m), a total of 37,500 m<sup>3</sup> would have been routed through the pond over this period. Even assuming the initial jump of 1.09 m is not due to water supply (detailed below), these figures suggest additional water supply from beyond the local catchment.

According to this back-of-the-envelope calculation, it is possible that water level rises at pond C and D in 2014, as well as J in 2013, occur due to local supply. However, the basic method has several important shortcomings beyond basic uncertainty in pond area and water supply. First, the response of pond water levels to events is not consistent between ponds or for any pond throughout the record. For instance, pond D shows a clear and immediate water level spike in response to precipitation in late May, but no obvious response to the many later precipitation events. If the pond is fed only by the local catchment over this period, it should respond in a similar way to comparable events. Second, the drops in water level after precipitation events are suggestive of drainage; these changes are too great to be accomplished by subaqueous melt. Third, the catchment area here is determined based on a 3 m barrier to surface flow, but the real local catchment areas may be much smaller as local sinks are extremely common on Lirung and other debris-covered glaciers, and debris-thickness observations greater than 2 m are rare (McCarthy et al., 2017). Finally, this method ignores the energy balance of the ponds, which indicates significant discharge and water supply even during drainage (Miles et al., 2016); this water supply is much more than can be derived from the local catchment.

## 2.2 Short-term changes

We now use the same framework to interpret various short-term changes, including jumps and diurnal variations in water level:

- *Pond C, 1 March 2014:* The pressure transducer at pond C measured a water level jump of 0.25 m on 1 March 2014 (Figure S8). There was no precipitation at the time, and daily air temperatures were below freezing. The sudden change (between 15-minute measurements) suggests a stochastic event such as boulder capture or calving rather than a brief pulse of water from upstream. We estimate a pond area of 325 m<sup>2</sup> based on the water level relative to the May 2014 UAV orthoimage, suggesting a volumetric change of 81 m<sup>3</sup> associated with the water level change, equivalent to a cube 4.3 m to a side. This could be explained by a single very large boulder capture (there are suitable specimens on the glacier) or a moderate calving event given the size of the ice cliff. It could also be explained by

debris slumping, but the event would have involved one or more large boulders and a large quantity of smaller clasts as well.

- *Pond I, 31 May 2014*: Diurnal variations are common throughout the water level records, so we assess a typical diurnal variation for pond I. On 31 May, the water level showed a rise of 0.04 m to peak at 13:00, before falling to yield a net decline of 0.01 m over the day (Figure 4). There was no precipitation, but the on-glacier temperature sensor recorded 7.4 PDD. Based on the local catchment area (29,772 m<sup>2</sup>), we estimate a meltwater supply of 163 m<sup>3</sup> during the day. As pond I's surface area remained steady during 2014, we assume a ponded area of 900 m<sup>2</sup>, which equates to a volume increase of 36 m<sup>3</sup> during the day, and a net loss of 7.2 m<sup>3</sup> over the day. Thus, the diurnal water level rise could be caused by the delivery of local meltwater (Benn et al., 2017; Horodyskyj, 2017). If the water level decline corresponds to basin expansion (rather than outflow discharge) this would equate to 72 m<sup>3</sup> of subaqueous melt during the day due to the density difference of ice and water. Miles et al. (2016) found a mean subaqueous melt rate of 0.029 m d<sup>-1</sup> for pond C in 2013. This rate would require a subaqueous surface area of 2,500 m<sup>2</sup>, or an average depth of 30 m along the edge of the pond bordering ice cliff (~ 80 m). This suggests that diurnal net water level lowering is likely too great to be attributable to subaqueous basin expansion alone. Importantly, this is the net decline, and the total decline of 0.05 m within the day is much too great to be accounted for by subaqueous melt, and strongly suggests that some discharge was leaving the pond.
- *Pond D, 22-27 May 2014*: A multiday spike over 26-28 May stands out in Pond D's water level record (Figure 4). This event is preceded by four days of precipitation, registering 37 mm, and moderate air temperature (33.3 PDD). With a catchment area of 19,400 m<sup>2</sup>, we estimate a local supply of 718 m<sup>3</sup> of precipitation and 478 m<sup>3</sup> of meltwater. This more than accounts for the 150 m<sup>3</sup> volume increase associated with the precipitation event. Notably, pond J shows a heightened water level increase on 25 May (0.23 m, 0.06 m greater than background rate), but neither pond I nor pond C show a response to this event.
- *Pond D, 2 August 2014*: Pond D's record exhibits a prominent jump of 0.43 m on 2 August, followed by a slow decay to the previous water level over several days (Figure 4). Given a pond surface area of ~ 500 m<sup>2</sup>, this equates to a volume increase of 215 m<sup>3</sup>, equivalent to a cube 6 m to a side. Thus, the water level jump could be due to the capture of one or more very large boulders immediately surrounding the pond (Figure S5).
- *Pond J, 21 April 2014*: The long water level rise of pond J in 2014 was initiated by a jump of 1.09 m (Figure 4). The pond's area at this time was ~4,000 m<sup>2</sup>, so this water level rise indicates a sudden displacement of 4,360 m<sup>3</sup>, which does not seem plausible for a debris slump. There is prior evidence

of subaerial calving at pond J, and this displacement would correspond to a block of 90x20x2.4 m. Collapse of the conduit draining the pond seems plausible, as this would explain the cutoff of water supply to pond C.

### 3 POND LEVEL LOWERING MECHANISMS

Slow water level lowering could be explained by three major mechanisms: englacial discharge by a low-slope spillway, seepage through a debris-filled conduit, or subaqueous ablation. We assess each of these possibilities based on back-of-the-envelope calculations. We find that steady spillway incision can only account for observed lowering rates if the spillway is steep ( $> 9\%$  gradient), that discharge through porous media cannot account for discharge rates during a moderate water level decline unless the gradient is 100% or greater, and that background subaqueous ablation is a plausible cause for the steady lowering.

#### 3.1 Spillway incision

One possibility is that a low-slope spillway enables water level lowering through slow incision. For this process, incision is controlled by channel gradient and discharge (e.g. Raymond and Nolan, 2000; Jarosch and Gudmundsson, 2012). Although this mechanism provides a positive feedback (more incision leads to more drainage) and can cause catastrophic drainage for supraglacial water bodies (e.g. Koziol et al., 2016), the small volumes of the study ponds are likely to limit water supply. In order to evaluate this possibility, we assess incision rates modelled for englacial conduits by Jarosch and Gudmundsson (2012). In Table S2 we compare select model runs to observations of englacial conduit gradient by Gulley et al. (2009), modelled discharge for pond C (Miles et al., 2016), and water level lowering rates measured in this study (presented in Table S4). We then scale the results of Jarosch and Gudmundsson (2012) for a plausible configuration at Lirung Glacier, using the (Miles et al., 2016) discharge rate and a 3% conduit gradient.

We find that the scaled incision rates for a 3% gradient are too low to account for most of the observed mean rates of water level lowering (excepting the latter period of 2014 for pond C). To achieve the water level lowering rates observed at ponds D and I in 2014, a spillway would need an average gradient of 9%, a value that is consistent with some cut-and-closure conduits, although these features usually have a lower gradient (Gulley et al., 2009). Using the most extreme englacial conduit gradient observed for similar glaciers (30%) yields an incision rate of  $0.12 \text{ m d}^{-1}$ , which is insufficient to account for the faster rates of water level decline. Consequently, this mechanism is possible for some slow declines if drainage occurs though a steep conduit, but incision cannot account for the major drainage events.

### 3.2 Debris-filled conduit

Another possible mechanism for low rates of water lowering is seepage through saturated debris. Although this process is likely to lead to increasing drainage efficiency, eventually forming a conduit (Gulley et al., 2009), it could explain slow water level decline for a short period. Miles et al. (2016) attributed the slow drainage of Pond C in 2013 to seepage through a debris-filled conduit, noting the emergence of a conduit within the pond's depression in 2014. That study calculated discharge rates for the pond based on diurnal heat storage variations, and determined a typical mean rate of  $0.028 \text{ m}^3 \text{ s}^{-1}$ .

It is difficult to make a robust comparison to flow through saturated media due to many unknown parameters, but flow in saturated media is given by Darcy's Law (Equation 1), relating the volumetric flow rate ( $Q$  [ $\text{m}^3 \text{ s}^{-1}$ ]) to permeability ( $\kappa$  [ $\text{m}^2$ ]), fluid viscosity ( $\mu$  [ $\text{Pa s}$ ]), and hydraulic gradient ( $\nabla P$  [dimensionless]). By convention, the ratio of permeability to viscosity is the hydraulic conductivity ( $K = \frac{\kappa}{\mu}$  [ $\text{m s}^{-1}$ ]). We estimate a cross-sectional area of  $0.25\text{-}2 \text{ m}^2$  based on the conduits observed on Lirung Glacier. For hydraulic conductivity of the debris matrix (which could also be partially-refrozen), we use values corresponding to gravel, ranging between  $3 \times 10^{-2}$  to  $3 \times 10^{-4} \text{ m s}^{-1}$  (Domenico and Schwartz, 1998). The conduit gradient is also unknown, but for this we test values corresponding to observed conduits on Himalayan glaciers (Gulley et al., 2009).

$$Q = -\frac{\kappa A}{\mu} \nabla P \quad (1)$$

Results of these example calculations are included in Table S3. Our discharge estimates are less than the mean discharge estimated by (Miles et al., 2016), which suggests a higher gradient, a larger channel, more conductive media, or possibly an incorrect estimate by that study. Of these, a higher gradient is very plausible, as locally-reduced drainage efficiency would impound water, leading to heightened hydraulic gradient through the blockage. The flow estimate for 100% gradient (which would correspond to a blockage length equal to the impounded water depth) with  $K = 0.03 \text{ m s}^{-1}$ , produces a flow estimate comparable to the discharge estimate of Miles et al. (2016). We therefore consider this a possibility for ponds maintaining inefficient connectivity to the endglacial drainage network.

### 3.3 Subaqueous ablation

Due to the density difference between ice and water, melt below the waterline leads to a greater increase in depression volume than the corresponding input of water. Consequently, prolonged subaqueous melt is another plausible mechanism of water level lowering. Using a methodology similar to the water source

investigations, we assess lowering rates from several records to determine whether this mechanism can account for the observed rates of change (Table S4).

Based on the orthoimages, we estimate a representative pond area and measure the length of ice cliff in contact with the pond for the relevant period. The mean rate of lowering corresponds to an average daily volumetric change. Based on the density difference of water and ice ( $\rho_i = 900 \text{ kg m}^3$ ), and a mean subaqueous melt rate of  $0.029 \text{ m d}^{-1}$  (Miles et al., 2016), we calculate the subaqueous area that would be required to account for the daily volume change. From this, and assuming a vertical subaqueous surface beneath the ice cliff, we calculate the mean depth of a subaqueous ice interface.

This method has moderate uncertainty, but clearly distinguishes between the steeper declines that cannot be explained by this mechanism (e.g. pond J, 2013; Figure 3) and the shallower declines that could be (e.g. pond I, 2014; Figure 4). The steeper declines cannot be attributed to subaqueous melt, as the subaqueous ice surfaces needed for melt are unrealistically large. The steeper declines can only be explained by drainage.

We specifically examine three periods in 2013 and two in 2014 for pond C, each with a steady rate of water level decline. In 2013, the water level first declined at a rate of  $0.015 \text{ m d}^{-1}$  (24 May to 19 June), then the rate increased to  $0.099 \text{ m d}^{-1}$  until 6 July, when the rate of decline dropped again (to  $0.053 \text{ m d}^{-1}$ ). The analysis shows that the water level decline may be explained solely by subaqueous melt during the first and third periods, but that drainage must have contributed to lowering during the second period; Miles et al. (2016) determined that the pond underwent slow discharge during the whole period based on the pond's energy budget, and our result here suggests that drainage was at least active for the middle period.

In 2014, pond C experienced a sharp decline of  $0.223 \text{ m d}^{-1}$  (following basin flooding) then a long period of gradual lowering at  $0.012 \text{ m d}^{-1}$  (Figure 4). Our analysis indicates that while subaqueous melt cannot account for the sharp decline (which is therefore certainly due to drainage), it can easily account for the rate of lowering observed between 1 May and 1 August. Importantly, while the magnitude of this process varies seasonally (Miles et al., 2016), it occurs at all ponds bordered by ice cliffs for the entire melt season.

## 4 POND-BY-POND OBSERVATIONS AND INTERPRETATION

Here we present the detailed observations of changes at each pond and our interpretation.

### 4.1 Pond C, 2013

Pond C was the most comprehensively observed pond on Lirung Glacier through instrumentation and field surveys (Figure S4). This pond was the focus of energy-balance modelling in Miles et al. (2016), and the adjacent ice cliff is Cliff 2 in Steiner et al. (2015); Buri et al. (2016b); Brun et al. (2016); Buri et al. (2016a). This small pond (up to  $640 \text{ m}^2$ , smaller than a Landsat pixel) was heavily shaded by a 20 m

high ice cliff during all four field visits (Figure 5). The ice cliff presented an overhanging, scalloped face directly above the ice-water contact, which retained a similar geometry over the study period as the cliff backwasted (Figure 5b,c). The ice cliff has been thoroughly investigated through stake measurements, photogrammetric surface reconstruction, and near-surface meteorological modelling (Steiner et al., 2015; Buri et al., 2016b; Brun et al., 2016; Buri et al., 2016a).

In 2013 the pond decreased in surface area between the May and October orthoimages from 640 m<sup>2</sup> to 380 m<sup>2</sup> (Figure 5a,d). This decrease in surface area was accompanied by a lateral translation of ~7 m in the direction of the adjacent ice cliff's backwasting, which differs in direction from the local glacier surface velocity of ~2 m a<sup>-1</sup> (Kraaijenbrink et al., 2016).

Between May and October, a net lowering of the pond's elevation of 3 m occurred (Figure 5b,c), a value higher than surface lowering of the nearby debris-covered areas (0.5-1.5 m Immerzeel et al., 2014a). Basin expansion during this period was dominated by backwasting of the adjacent ice-cliff (Figure 5b,c). After the monsoon season, the perched pond primarily occupied the area of very high surface elevation change (Figure 5d), corresponding to the prior position of the ice cliff. A substantial deposition of debris occurred at about the position of the overhanging ice cliff's lip, the point of debris supply as the ice cliff backwasted, fundamentally changing the depression geometry and bounding the ponded area (Figure 5b-c).

The pressure transducer at pond C initially showed a stable water level, then documented a gradual water lowering of 2.32 m over 44 days before subaerial exposure on 14 July (Figure 3). The water level record is characterised by diurnal fluctuations of 0.05 m with a peak at about 13:00, and occasional jumps or drops of up to 0.15 m. Over the period, pond-bottom water temperature fluctuated between 0.5°C and 1.5°C.

### *Interpretation*

The dates of water level decline initiation (25 May) and acceleration (20 June) indicate changes in the pond's internal dynamics. The first date corresponds to the start of significant subaqueous melt (outpacing water inputs) when the pond temperature increases around 25 May. The second transition suggests an increase in drainage efficiency beginning 20 June, which leads to a slow, steady water level decline and a significant decrease in ponded area by October 2013. Thus, in 2013 pond C shows water level lowering associated with subaqueous melt followed by slow drainage (Miles et al., 2016).

## **4.2 Pond C, 2014**

According to the 21 April 2014 SPOT6 orthoimage, the pond's area had increased to 950 m<sup>2</sup>, but the ponded area decreased to 220 m<sup>2</sup> by 1 May 2014. The ponded area increased slightly to 340 m<sup>2</sup> in November. As in 2013, the pond area changes were accompanied by a lateral translation between May 2014 and November 2014 of the pond outline of ~5 m, again in the direction of ice cliff backwasting (Figure

5a,e). Based on the DEMs, the pond showed net surface lowering of  $\sim 1$  m between October 2013 and May 2014, and a further  $\sim 3.5$  m by November 2014. As in 2013, basin expansion during 2014 was dominated by backwasting of the adjacent ice-cliff; in the post-monsoon the perched pond primarily occupied the area of very high surface elevation change, and significant debris deposition occurred in this zone (Figure 5b,c,e).

The pressure record for pond C was continuous from October 2013 until the water level dropped below the sensor in late July 2014 (Table 1). In winter 2013-2014, the pond's basal water temperature dropped to  $0^{\circ}\text{C}$  and at-sensor pressure increased before stabilizing at 1.4 m water depth. Diurnal fluctuations are very weak ( $< 0.02$  m) for most of the winter, but a small jump in water depth (0.25 m, equivalent to a displacement of  $\sim 80\text{ m}^3$ ) occurred on 1 March, at which point the diurnal oscillations strengthened to  $\sim 0.05$  m (Figure 4). Water level began to rise on 15 March, and pond-bottom temperatures increased to  $1\text{-}2^{\circ}\text{C}$ . Water level rose by 1.77 m over 38 days to peak on 21 April, then lowered by 2.23 m over 10 days. After 1 May, water level resumed gradual lowering ( $\sim 0.2$  m per month) for the remainder of the monsoon. The water level record for this period shows diurnal fluctuations of 0.02-0.05 m, and one large drop of 0.3 m occurred on June 8-9. During the field visit in May 2014, a small surface stream was observed meandering to an englacial conduit opening (position indicated on Figure 5).

The pond water level fluctuations and basin elevation profiles demonstrate a continuous overall decline in the elevation of the water surface as the nearby ice-cliff backwasted (Figure 5). The magnitude of this decline ( $\sim 8$  m) was greater than local surface change ( $\sim 0\text{-}3$  m) and greater in each year than the water level decline observed by pressure transducers, but those records do not encompass the entire monsoon due to subaerial exposure.

### *Interpretation*

The decline in water temperature, elimination of diurnal fluctuations, and stabilization of water level during the winter period correspond to pond freeze-over and snow overburden (Figure 3c). The reinitiation of diurnal fluctuations suggests reconnection to water input and outflow discharge paths, and the broad rise and fall in water level clearly represents a significant change in the balance between water inputs and outflow discharge, flooding the local depression. A steady decline occurs after the impounded water leaves the system. Thus, in 2014 the pond shows a filling and drainage event, followed by the lowering effect of subaqueous melt.

The conduit opening found at pond C in May 2014 may have been an englacial void or conduit during 2013. This position was behind the ice-cliff and beneath several meters of ice, but had been exposed subaerially due to surface thinning and ice-cliff backwasting. The opening may have established an efficient connection to the englacial and subglacial drainage network, enabling a faster drainage in late April 2014

than the previous year. At the time of the visit, however, water was routed away from the pond through a series of small pools in the debris (Figure 5) to spill into this small hole. Consequently, the hole's position, rather than conduit size, limited the pond's drainage, so the positive feedback mechanisms of pond drainage (Gulley et al., 2009) were not operating, and the drainage and water level decline progressed slowly after 1 May.

### 4.3 Pond D, 2013

Pond D appeared to be a small, stagnant perched pond in 2013 and was surrounded only by debris slopes of about 20° inclination; it was not investigated in detail (Figure S5). The 2013 orthoimages show only very slight differences in ponded area (Table 3) and outline (Figure 6a,d), with little indication of pond translation. There was no change in pond elevation in 2013, and very slight basin expansion along the marginal debris slopes (Figure 6b,c,d).

#### *Interpretation*

The few changes observed at pond D in 2013 suggest that the feature was entirely disconnected from the rest of the glacier's drainage network.

### 4.4 Pond D, 2014

In the April 2014 SPOT6 orthoimage, the ponded area had expanded to 500 m<sup>2</sup>, and the ponded area in May was very similar in coverage, although the higher resolution of the UAV orthomosaic indicated numerous boulder islands. The April and May 2014 orthoimages also indicated that several ice cliffs had emerged around the pond. By November 2014, the pond had fragmented into four small water bodies, separated by a large debris mound, and covering a total area of 160 m<sup>2</sup> (Figure 6a,e). One of the pond segments occupied the pond's earlier position, but a different segment had shifted ~ 10 m to the south, occupying a space previously beneath a debris slope.

The May 2014 DEM shows the pond water level ~1 m lower than in May and October of 2013, but the water level lowered a further ~5 m between May and November 2014 (Figure 6b,c). The pond's depression expanded on all sides during this period. A single large ice cliff emerged on the pond's southern margin, while the other sections of ice exposed in May 2014 were re-buried by debris; the reburied ice cliff slopes exhibited a shallower slope than the remaining cliff face. The large ice cliff developed a distinct thermo-erosional notch at about the May 2014 water level. Beneath one section of this cliff, flowing water could be heard in October and November 2014 (position indicated on Figure 6a,c).

A pressure transducer was installed in pond D on 5 May 2014 (Table 1). The water level rose 1.07 m in the 44 days after pressure transducer installation to peak on 18 June (Figure 4). The water level then

dropped 2.25 m over the next 70 days. The water level dropped below the pressure transducer on 28 August, at which point the water level was declining at a rate of  $\sim 1$  m per month. Water level fluctuated erratically over the entire period, with sharp drops or rises of up to 0.51 m superimposed over background diurnal fluctuations of 0.07 m. Pond-bottom temperature ranged between 0.8°C and 2.5°C over the observation period.

### *Interpretation*

In 2014, pond D exhibited an overall water level rise followed by a decline, encompassing a period when the pond experienced significant basin expansion and pond shrinkage. The unsteady water level rise is interpreted to be due to net water influx until 15 June, when a change in the water balance or increased basin expansion led to a general water level decline. This decline was gentle and can be attributed to subaqueous melt and basin expansion rather than pond drainage alone. The presence of audible flowing water and the exposure of a conduit segment (both observed in November 2014) is evidence of connection to the englacial drainage system at that water level. The pond water level declined 5 m between May and November, but the water level record accounts for only 1 m net decline by mid-August, suggesting a later partial drainage and/or surface subsidence related to the collapse of englacial voids. Either process would be associated with connection to an englacial drainage pathway.

The pressure transducer record was characterised by sudden changes in water level. Sharp rises are likely due to the capture of several very large boulders during basin expansion, which would displace a significant volume for the small pond. Significant amounts of debris were relocated to the depression's center (Figure 6b,c), dividing the pond into three distinct water bodies, although it is probable that they were hydraulically connected through saturated debris. The sharp drops most likely correspond to surface subsidence in the pond depression as englacial voids collapsed (Mertes et al., 2016).

## **4.5 Pond I, 2013**

Pond I (Figure S6) was not observed in detail in May 2013, but appeared in the UAV orthophoto as a pond of moderate size (740 m<sup>2</sup>, possibly observable by Landsat) with an adjacent ice cliff with a fairly uniform slope angle, and no vertical or overhanging face (Figure 7a,b,c). The adjacent ice cliff was investigated by Brun et al. (2016); Buri et al. (2016a) and was designated Cliff 4. The pond shrunk slightly in area to 550 m<sup>2</sup> by October 2013 (Figure 7), and the pond outline translated  $\sim 10.5$  m to the east (local glacier surface velocity is  $\sim 3$  m a<sup>-1</sup> to the southeast). During this period, however, the water surface lowered  $\sim 8$  m, revealing a 4 m vertical section at the base of the cliff (Figure 7b,c).

The pond basin expanded between May and October 2013, primarily due to ablation of the adjacent ice cliff. This ice cliff also expanded dramatically, extending west (Brun et al., 2016). This new band of ice

cliff had a relict englacial conduit at its base, occupying a zone between the May and October 2013 pond levels, and exhibited a parallel debris mound with apex near the prior slope (Figure 7b,c,d).

### *Interpretation*

Pond I experienced moderate changes in basin geometry in 2013, associated with a strong net water level lowering, ponded area decrease, a change in the ice cliff's appearance, and the emergence of the relict conduit segment through roof collapse. The high water level in May 2013 indicates that the depression was flooded prior to the May 2013 visit, submerging any thermo-erosional notches. Water-level lowering during 2013 decreased the pond's surface area, exposing thermo-erosional notches, previously-subaqueous vertical segments of the ice cliff, and the englacial conduit.

The water level lowering was accomplished by the combination of subaqueous ablation and partial englacial drainage, as the exposed conduit segment was between the May and October water levels. As the exposed conduit segment was immediately down-glacier and at a slightly lower elevation than pond J, it may have been associated with that pond's observed drainage in July 2013 (Figure 3b). This would have led to englacial ablation near the pond's confining ice-cliff, and may have established an efficient drainage path at that level.

## **4.6 Pond I, 2014**

In April 2014, pond I had a surface area of 880 m<sup>2</sup>. The pond was not within the UAV survey area for May 2014, but in November 2014 it had grown slightly to an area of 990 m<sup>2</sup> (Figure 7a,e). The pond outline translated to the east ~ 7.5 m between October 2013 and November 2014 (Figure 7e).

The April 2014 DEM is not of comparable quality to the UAV and terrestrial SfM DEMs, but between October 2013 and November 2014 pond I's water level lowered ~5 m (Figure 7b,c). During this period, the basin expanded due to ice cliff backwasting at the pond's eastern margin (as in 2013) and to the southwest of the pond, associated with the newly-exposed ice cliff and conduit segment (Figure 7b,c,e). The area of this conduit visible at the surface had expanded, revealing additional openings and progressively exposing additional bends (Figure 9c). The adjacent debris mound, a location of enhanced surface lowering in 2013, instead showed minimal surface lowering (Figure 7d,e).

Pond I was also monitored with a pressure transducer from 8 May to 18 August 2014 (Figure 4). The pond surface continuously lowered for the entire period of record (103 days), a total change of 3.58 m before subaerial exposure. The water level record shows diurnal fluctuation of ~ 0.04 m, with several spikes up to ~ 0.2 m, and pond-bottom temperature was between 0.5°C and 2.5°C.

### *Interpretation*

In 2014, pond I maintained its area but the water level gradually declined. The slow rate of water level lowering was due to subaqueous melt, rather than drainage. The pond lost its efficient drainage path due to sustained water level lowering (15 m between May 2013 and October 2014).

#### 4.7 Pond J, 2013

Pond J was the largest pond-cliff system observed on Lirung Glacier during the study period, and exhibited major fluctuations in area, but covered a greater area in the pre-monsoon for both years (Figure S7). The adjacent ice cliff was investigated by Brun et al. (2016) and was designated Cliff 5. The pond has two sections, which were initially divided in May 2013 by an ice dam. At this point the ponded area encompassed 7,290 m<sup>2</sup> (many Landsat pixels); by October 2013 the pond had reduced in area to 450 m<sup>2</sup> and occupied two small depressions to the southwest. This remaining ponded area had been translated ~10m to the southeast through the combination of glacier surface velocity ( $\sim 4\text{m a}^{-1}$ ; Kraaijenbrink et al., 2016) and ice cliff backwasting ( $\sim 6\text{m a}^{-1}$ ; Brun et al., 2016).

Pond J is located at the boundary of the UAV survey area, and we have lower confidence in the geometric accuracy of the UAV DEMs here. The pond's water level was observed with a pressure transducer from 11 May until subaerial exposure on 23 June 2013 (Table 1). During this period, the water level initially rose 1.2 m over 28 days before a period of stability, then lowered 2.8 m over 13 days (Figure 3). The water level fluctuated diurnally by  $\sim 0.035$  m, and the sensor recorded several jumps of up to 0.18 m. During the observation period, pond temperature ranged between 0.7°C and 2.2°C.

The drainage of the eastern half of pond J by October 2013 revealed a well-preserved englacial conduit floor at the base of the large ice cliff with false floors (similar to those described by Gulley and Benn, 2007; Benn et al., 2009) and multiple lateral thermo-erosional incisions at the outer margin of conduit meanders (Figure 9a). Emerging from the debris surface within the depression, the conduit was 2 m wide and extended for 40 m along the cliff's base before entering a zone of debris deposition due to the ice cliff's backwasting (Figure 8).

##### *Interpretation*

For pond J in 2013, water inputs outpaced subaqueous melt until 31 May, when a balance was reached. The sudden rises in water level on 9 and 10 June represent significant, instantaneous volume inputs given the pond's size, most likely associated with either boulder capture, debris slumping or calving. The gradual decline in water level (11-15 June) suggests that subaqueous basin expansion was outpacing water inputs. Pond drainage then began on 15 June when an efficient connection was established with the englacial network, and the pond's drainage likely led to downglacier surface subsidence associated with the structural collapse of the conduit exposed at pond I.

## 4.8 Pond J, 2014

In April 2014 pond J had an area of 3,980 m<sup>2</sup>, again encompassing both depressions and spanning nearly the complete width of the glacier tongue, but in November 2014 the pond's area had declined to 1,570 m<sup>2</sup>, and occupied the northeast depression (Figure 8). This pond edge had shifted to the southeast by ~20 m since May 2013.

The pressure transducer at pond J (reinstalled 25 October 2013) recorded a steady water level for most of the winter, and the pond's basal water temperature slowly dropped to 0°C (Figure 4). Water temperature began to rise on 6 April, then water level suddenly rose by 1.23 m on 21 April. This was followed by a steady, uninterrupted rise of 4.9 m over the next 48 days, with pond-bottom temperatures ranging from 1.0°C to 2.5°C during the water level rise. The high water level in May 2014 prevented access to the water level logger for data download and reinitialization, so the data-logger ran out of memory on 8 June, before the pond's drainage.

After the pond's drainage, field surveys in October and November of 2014 again discovered relict conduits exposed at the surface leading into the western pond depression from up-glacier (Figure 9d).

### *Interpretation*

As at pond C, the decline in water temperature, elimination of diurnal fluctuations, and stabilization of water level during the winter period indicate pond freeze-over and snow overburden (Figure 3f). Although at its smallest extent in October 2013, the pond has a significant thermal storage capacity and maintains positive pond-bottom water temperatures until late January. The observed temperature increase in early April is due to the pond surface thawing. In mid-April, the sudden rise in water level is immediately followed by sustained flooding, accounting for at least 6 m of water level rise, suggesting a structural change that also resulted in water routed into the depression.

This sudden change is precisely aligned with the peak of pond C's water level in the afternoon of 21 April (Figure 4). Subsequently, the pond C water level dropped over ten days (estimated pond volume change of 1600 m<sup>3</sup> based on the May 2014 DEM) before switching into a gradual decline, while pond J's volume increased by an estimated 6000 m<sup>3</sup> over the following day, and experienced continuous water level increase until at least June. We interpret this behaviour as a reconfiguration in the drainage network (i.e. collapse of an active conduit segment between the two ponds) on 21 April which initiated the backup of water in pond J, and cut off the supply of water to pond C, allowing it to drain until reaching a local hydraulic table.

The datalogger stopped recording in early June, and pond J drained before our return in October. This pond captured nearly all surface and shallow-englacial flows until its drainage; the deep basin extends across much of the glacier width. Due to the complete drainage of this pond section, we expect that drainage

occurred by sudden connection to a pre-existing conduit. The magnitude of flooding and timing of drainage are not known precisely, but the release of this stored water and heat is likely to have caused major changes to the down-glacier drainage network (Benn et al., 2012; Miles et al., 2016; Rounce et al., 2017). Given the position of this drainage point, the drained water may have followed the glacier's true right side (i.e. approximately following path D2 rather than D1 in Figure 12). The pronounced changes between May and November at pond D could be an expression of this drainage.

## 5 MECHANISMS OF ENGLACIAL CONDUIT EXPOSURE

Relict englacial conduits were exposed at the glacier surface in a variety of locations throughout the study period. The relict conduits had usually experienced roof collapse, although some sections presented weak natural arches.

The evidence suggests that the relict conduits were exposed via at least three mechanisms. The first is exemplified by the segments of relict conduits exposed at pond J (Figure 9a,d). Here, a decline in pond water level exposed the conduits in both years. These conduit segments always had only a single wall, rather than a complete conduit tunnel structure. The segments were often leading into the pond depression from up-glacier (indicative of englacial supply to pond depressions), and in one case found along the base of the ice cliff confining the depression (indicative of down-glacier discharge from the ponds).

The second conduit exposure mechanism is ice cliff backwasting. This is exemplified by relict conduits adjacent to ponds A, C, D, and I (Figure 9b). These conduits had a complete tunnel structure, presenting a single circular opening. They appeared in various locations across several ice cliffs; at the base, elevated off the pond floor, or intersecting the cliff in multiple locations. The shape of these conduit openings seems to be the result of the intersection between a planar ice face and a sinuous conduit passage. If and when such conduits intersect the depression base, these features would lead to complete pond drainage, while other positions on the ice cliff would lead to partial drainage. Depending on the local hydraulic gradient, conduits could also lead to pond filling.

The third conduit exposure mechanism is structural collapse of a conduit roof (e.g. Kirkbride, 1993; Sakai et al., 2000; Benn et al., 2012). The clearest case of this process occurred near pond I between May and October 2013 (Figure 7), although a similar process occurred for pond D between May and October 2014 (Figure 6). In both cases, the depression expanded dramatically. Prior to the changes, neither pond exhibited a large ice cliff, but afterwards they had a large continuous ice cliff on one side and a debris hummock parallel to it within the depression.

## 6 OBSERVATIONS OF THERMO-EROSIONAL NOTCHES

The repeat field visits to Lirung Glacier enabled various other pond-related phenomena to be observed. Although we did not take rigorous measurements of them in this study (see Benn et al., 2001; Röhl, 2008) they offer basic evidence of the mechanisms by which supraglacial ponds affect the debris-covered surface.

Thermo-erosional notches were observed at most ponds with marginal ice cliffs in the study area, regardless of pond area or depression depth. Subaerially-exposed notches extended a few metres, similar to the observations of Röhl (2006). Notches have been observed to extend much greater distances on other glaciers (Xin et al., 2011).

Two types of notch were observed. First, a series of horizontal waterline scars was observed on pond C (Figure S10a; discussed in Miles et al., 2016). They were only observed at pond C in 2013, and they were subaerially modified over subsequent days. Based on the pressure transducer data, the features seem to align with brief periods of stability in the lowering water level. They are interpreted, therefore, as evidence of the peak diurnal melt rates during the pond's slow drainage, when the subaqueous melt rate exceeds the subaerial melt rate. The brief period of diurnal water level stability corresponds to a temporary balance between inputs, outputs, and basin expansion.

The second, more common notch type exhibited a single lip with a horizontal roof near the waterline, extending under the ice cliff an unknown distance. These notches are most apparent when the water level is below the notch (Figure S10b) but notches are also often identifiable very close to waterlines (Figure S10c-d). These notches are interpreted to form over long periods of stable water level, when water supply to the pond is equal to the subaqueous basin expansion and outflow.

Thermo-erosional melting can lead to calving at supraglacial ponds (Benn et al., 2001; Diolaiuti et al., 2005; Benn et al., 2007; Sakai et al., 2009). Of the four ponds observed in detail, only pond J had sufficient fetch to be conducive to calving (Sakai et al., 2009). This pond exhibited signs of calving, including enlarging fractures at its marginal ice cliff (regularly observed, e.g. Figure S7b) and floating irregular ice blocks within the pond (observed in May 2013).

## 7 UNCERTAINTY OF DEM-BASED WATER LEVEL CHANGE

Here we provide a brief assessment of the propagation of uncertainties associated with the measurement of water level changes from the SfM DEMs used in this study.

Water level is measured from the DEMs as the mean of elevation values within the delineated pond area; these values are statistically in agreement within the uncertainty of the SfM data. To determine a change in pond level from the observed elevation changes, it is necessary to account for this DEM uncertainty,

as well as the glacier's slope and emergence velocity. These values are related by simple addition, so the propagated uncertainty is given by quadrature (root-sum-squared of the individual uncertainties), and we can assess this for ponds C, D, and I in 2013.

For these calculations, we use the surface displacements measured by Immerzeel et al. (2014b) for May-October 2013, which corresponds to our monsoon observation period, and the glacier's average surface gradient across the survey area of  $\sim 6^\circ$ . These can be combined to estimate the uncertainty of elevation change due to the glacier's basal slope. Lirung typically exhibits very small emergence velocities, typically  $< 0.2 \text{ m a}^{-1}$  (Naito et al., 1998; Immerzeel et al., 2014b), but Immerzeel et al. (2014b) infer a localised positive emergence velocity in the region of ponds C and D, of up to a maximum of  $\sim 0.5 \text{ m}$  between May-October 2013. The SfM DEMs themselves are generally accurate to 0.5 m vertically (Immerzeel et al., 2014b; Brun et al., 2015), and each change observation requires two independent SfM DEMs.

Surface displacements for May-October 2013 were  $\sim 1.5 \text{ m}$  in the area of pond C, giving  $\sim 0.17 \text{ m}$  elevation change due to mean slope. The observed elevation change for pond C's surface was 3.1 m, and we assume uncertainty in emergence velocity of 0.5 m. Via quadrature, this gives an uncertainty of surface elevation change of 0.9 m for pond C. Thus, the observed 3.1 m surface lowering in 2013 is greater than the uncertainty, reflecting a real change in water level. The pond's water level lowered by 3.5 m between May and November 2014. The November terrestrial SfM DEM has a higher vertical uncertainty of 1.0 m, leading to an uncertainty of surface elevation change of 1.23 m for the 2014 period, and again indicating a real water level change.

Pond D is subjected to the same displacement and emergence velocity as pond C, leading to the same uncertainty for 2013 (0.9 m) and 2014 (1.23 m), but exhibits a negligible elevation difference for May-October 2013. Consequently, it cannot be determined from the DEMs if the water level changed over this period. For May-November 2014, a 5.0 m change in water level was measured, exceeding the measurement uncertainty.

Surface velocities are higher at pond I, leading to a 2013 May-October displacement of  $\sim 2.5 \text{ m}$ . This produces up to 0.3 m change due to mean slope. As this pond is outside the zone of heightened emergence velocity, we assume the background emergence velocity is up to 0.2 m. This produces an uncertainty of surface elevation change of 0.8 m for 2013 and 1.2 m for 2014. The DEMs show a pond elevation decline of 7.2 m in 2013 and another 5.0 m in 2014, both beyond the measurement uncertainty.

## REFERENCES

Benn, D., Bolch, T., Hands, K., Gulley, J., Luckman, a., Nicholson, L., et al. (2012). Response of debris-covered glaciers in the Mount Everest region to recent warming, and implications for outburst

- flood hazards. *Earth-Science Reviews* 114, 156–174. doi:10.1016/j.earscirev.2012.03.008
- Benn, D., Gulley, J., Luckman, A., Adamek, A., and Glowacki, P. S. (2009). Englacial drainage systems formed by hydrologically driven crevasse propagation. *Journal of Glaciology* 55, 513–523. doi:10.3189/002214309788816669
- Benn, D. I., Thompson, S., Gulley, J., Mertes, J., Luckman, A., and Nicholson, L. (2017). Structure and evolution of the drainage system of a Himalayan debris-covered glacier, and its relationship with patterns of mass loss. *The Cryosphere Discussions* , 1–43doi:10.5194/tc-2017-29
- Benn, D. I., Warren, C. R., and Mottram, R. H. (2007). Calving processes and the dynamics of calving glaciers. *Earth-Science Reviews* 82, 143–179. doi:10.1016/j.earscirev.2007.02.002
- Benn, D. I., Wiseman, S., and Hands, K. A. (2001). Growth and drainage of supraglacial lakes on debris-mantled Ngozumpa Glacier, Khumbu Himal, Nepal. *Journal of Glaciology* 47, 626–638. doi:10.3189/172756501781831729
- Brun, F., Buri, P., Miles, E. S., Wagnon, P., Steiner, J. F., Berthier, E., et al. (2016). Quantifying volume loss from ice cliffs on debris-covered glaciers using high resolution terrestrial and aerial photogrammetry. *Journal of Glaciology* 62, 684–695. doi:10.1017/jog.2016.54
- Brun, F., Dumont, M., Wagnon, P., Berthier, E., Azam, M. F., Shea, J. M., et al. (2015). Seasonal changes in surface albedo of Himalayan glaciers from MODIS data and links with the annual mass balance. *Cryosphere* 9, 341–355. doi:10.5194/tc-9-341-2015
- Buri, P., Miles, E. S., Steiner, J. F., Immerzeel, W., Wagnon, P., Pellicciotti, F., et al. (2016a). A physically-based 3D model of ice cliff evolution on a debris-covered glacier. *Journal of Geophysical Research: Earth Surface* 121, 2471–2493. doi:10.1002/2016JF004039
- Buri, P., Pellicciotti, F., Steiner, J. F., Miles, E. S., Immerzeel, W. W., Evan, S., et al. (2016b). A grid-based model of backwasting of supraglacial ice cliffs on debris-covered glaciers. *Annals of Glaciology* 57, 199–211. doi:10.3189/2016AoG71A059
- Diolaiuti, G., Kirkbride, M. P., Smiraglia, C., Benn, D. I., D'Agata, C., and Nicholson, L. (2005). Calving processes and lake evolution at Miage glacier, Mont Blanc, Italian Alps. *Annals of Glaciology* 40, 207–214. doi:10.3189/172756405781813690
- Domenico, P. A. and Schwartz, F. W. (1998). *Physical and Chemical Hydrogeology* (Chichester, West Sussex, England: John Wiley & Sons), 2nd edn.
- Gulley, J. and Benn, D. (2007). Structural control of englacial drainage systems in Himalayan debris-covered glaciers. *Journal of Glaciology* 53, 399–412. doi:10.3189/002214307783258378
- Gulley, J. D., Benn, D. I., Sreaton, E., and Martin, J. (2009). Mechanisms of englacial conduit formation and their implications for subglacial recharge. *Quaternary Science Reviews* 28, 1984–1999. doi:10.1016/j.quascirev.2009.04.002

- Horodyskyj, U. (2017). Thermal and Physical Investigations into Lake Deepening Processes on Spillway Lake, Ngozumpa Glacier, Nepal. *Water* 9, 362. doi:10.3390/w9050362
- Immerzeel, W., Kraaijenbrink, P., Shea, J., Shrestha, A., Pellicciotti, F., Bierkens, M., et al. (2014a). High-resolution monitoring of Himalayan glacier dynamics using unmanned aerial vehicles. *Remote Sensing of Environment* 150, 93–103. doi:10.1016/j.rse.2014.04.025
- Immerzeel, W. W., Petersen, L., Ragettli, S., and Pellicciotti, F. (2014b). The importance of observed gradients of air temperature and precipitation for modeling runoff from a glacierized watershed in the Nepalese Himalayas. *Water Resources Research* 50, 2212–2226. doi:10.1002/2012WR013085. Received
- Jarosch, A. H. and Gudmundsson, M. T. (2012). A numerical model for meltwater channel evolution in glaciers. *The Cryosphere* 6, 493–503. doi:10.5194/tc-6-493-2012
- Kirkbride, M. P. (1993). The temporal significance of transitions from melting to calving termini at glaciers in the central Southern Alps of New Zealand. *The Holocene* 3, 232–240. doi:10.1177/095968369300300305
- Koziol, C., Arnold, N. S., Pope, A., and Colgan, W. (2016). Quantifying supraglacial meltwater pathways in the Paakitsoq Region, West Greenland. *Journal of Glaciology* , 1–13doi:10.1017/jog.2017.5
- Kraaijenbrink, P., Meijer, S. W., Shea, J. M., Pellicciotti, F., Jong, S. M. D. E., and Immerzeel, W. W. (2016). Seasonal surface velocities of a Himalayan glacier derived by automated correlation of unmanned aerial vehicle imagery. *Annals of Glaciology* 57, 103–113. doi:10.3189/2016AoG71A072
- McCarthy, M., Pritchard, H., Willis, I., and King, E. (2017). Ground-penetrating radar measurements of debris thickness on Lirung Glacier, Nepal. *Journal of Glaciology* 63, 1–13. doi:10.1017/jog.2017.18
- Mertes, J. R., Thompson, S. S., Booth, A. D., Gulley, J. D., and Benn, D. I. (2016). A conceptual model of supra-glacial lake formation on debris-covered glaciers based on GPR facies analysis. *Earth Surface Processes and Landforms* doi:10.1002/esp.4068
- Miles, E. S., Pellicciotti, F., Willis, I. C., Steiner, J. F., Buri, P., and Arnold, N. S. (2016). Refined energy-balance modelling of a supraglacial pond, Langtang Khola, Nepal. *Annals of Glaciology* 57, 29–40. doi:10.3189/2016AoG71A421
- Naito, N., Nakawo, M., Aoki, T., Asahi, K., Fujita, K., Sakai, A., et al. (1998). Surface flow on the ablation area of the Lirung Glacier in Langtang Valley, Nepal Himalayas. *Bulletin of glacier research* 16, 67–73
- Ragettli, S., Bolch, T., and Pellicciotti, F. (2016). Heterogeneous glacier thinning patterns over the last 40 years in Langtang Himal. *The Cryosphere* 10, 2075–2097. doi:10.5194/tc-2016-25
- Ragettli, S., Pellicciotti, F., Immerzeel, W. W., Miles, E. S., Petersen, L., Heynen, M., et al. (2015). Unraveling the hydrology of a Himalayan catchment through integration of high resolution in situ data and remote sensing with an advanced simulation model. *Advances in Water Resources* 78, 94–111. doi:http://dx.doi.org/10.1016/j.advwatres.2015.01.013

- Raymond, C. F. C. and Nolan, M. (2000). Drainage of a glacial lake through an ice spillway. In *IAHS Symposium: Debris-Covered Glaciers*. 264, 199–210
- Röhl, K. (2006). Thermo-erosional notch development at fresh-water-calving Tasman Glacier, New Zealand. *Journal of Glaciology* 52, 203–213
- Röhl, K. (2008). Characteristics and evolution of supraglacial ponds on debris-covered Tasman Glacier, New Zealand. *Journal of Glaciology* 54, 867–880. doi:10.3189/002214308787779861
- Rounce, D. R., Byers, A. C., Byers, E. A., and McKinney, D. C. (2017). Brief Communications: Observations of a Glacier Outburst Flood from Lhotse Glacier, Everest Area, Nepal. *The Cryosphere* 11, 443–449. doi:10.5194/tc-11-443-2017
- Sakai, A., Nishimura, K., Kadota, T., and Takeuchi, N. (2009). Onset of calving at supraglacial lakes on debris-covered glaciers of the Nepal Himalaya. *Journal of Glaciology* 55, 909–917. doi:10.3189/002214309790152555
- Sakai, A., Takeuchi, N., Fujita, K., and Nakawo, M. (2000). Role of supraglacial ponds in the ablation process of a debris-covered glacier in the Nepal Himalayas. In *Debris-Covered Glaciers*. 264, 119–130
- Steiner, J. F., Pellicciotti, F., Buri, P., Miles, E. S., Immerzeel, W. W., and Reid, T. D. (2015). Modelling ice-cliff backwasting on a debris-covered glacier in the Nepalese Himalaya. *Journal of Glaciology* 61, 889–907. doi:10.3189/2015JoG14J194
- Xin, W., Shiyin, L., Han, H., Jian, W., and Qiao, L. (2011). Thermal regime of a supraglacial lake on the debris-covered Koxkar Glacier, southwest Tianshan, China. *Environmental Earth Sciences* 67, 175–183. doi:10.1007/s12665-011-1490-1

## 8 SUPPLEMENTARY FIGURES

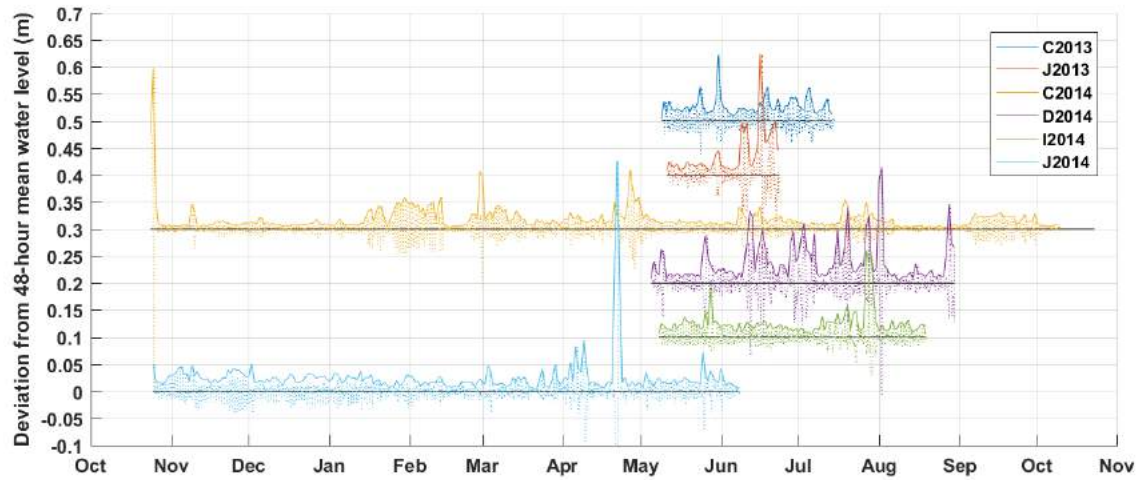


**Figure S1.** Magnitude of diurnal fluctuations at each pond, determined as the maximum daily deviation from a running 48-hour mean. 2013 and 2014 data are shown on the same time scale and baselines are elevated by 0.01 m increments for clarity. Values over 0.1 m correspond to jumps or drops in water level, rather than diurnal fluctuations.

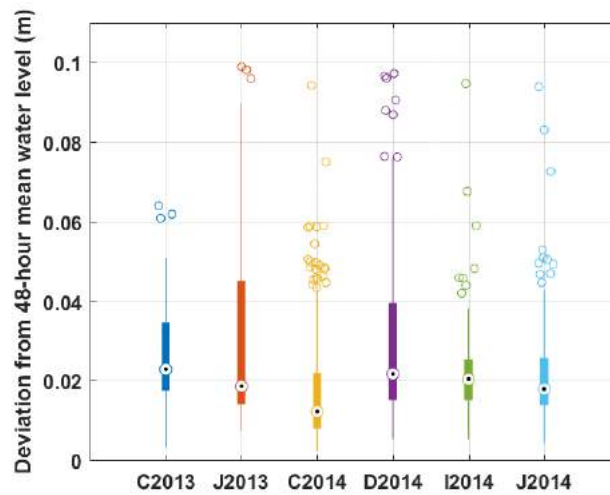


**Figure S2.** Box plots of diurnal fluctuation magnitude at each pond.

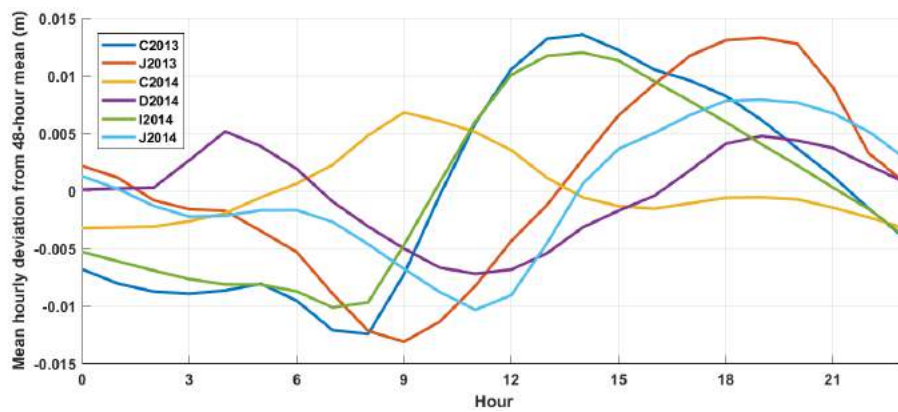


**Figure S3.** The average diurnal cycle for each pond. Ponds exhibit considerable variability in peak timing and curve shape.



**Figure S4.** Pond C in (a) May 2013, (b) October 2013, (c) May 2014, and (d) October 2014, showing ice-cliff retreat during the monsoon in each year. Drainage occurred prior to the field visit in May 2014 (c). A snowstorm immediately preceded the field visit in October 2014, blanketing the ice cliff and depositing a thick layer of wetted snow on the pond surface. Approximate photograph position indicated on Figure 3.



**Figure S5.** Pond D in (a) May 2013, (b) May 2014, and (c) October 2014, showing sudden depression expansion and water level decline in 2014. No suitable photograph was available for comparison from October 2013. Approximate photograph position indicated on Figure 5.



**Figure S6.** Pond I in (a) October 2013, (b) May 2014, and (c) October 2014. The cliff-pond morphology was very stable for this pond, although the whole system shifted position through melt and glacier flow. No suitable photograph was available for comparison from May 2013. Approximate photograph position indicated on Figure 6.

## 9 SUPPLEMENTARY TABLES

**Table S1.** Back-of-the-envelope calculations of local water supply and volumetric changes for selected events, including major seasonal rises (top four rows) and short-term changes (bottom rows). Precipitation is measured at the Kyanjing AWS, and PDD corresponds to the positive degree-days observed at the on-glacier air temperature logger. Melt is calculated from the mean degree-day factor of  $0.74 \text{ mm d}^{-1} \text{ }^{\circ}\text{C}^{-1}$  identified by (Immerzeel et al., 2014a). All volumes are in water-equivalent.

Pond	Year	Start	End	Period of water level rise			Estimated area ( $\text{m}^2$ )		Head gain (m)		Local inputs ( $\text{m}^3$ )		Pond volume change ( $\text{m}^3$ )	
				Duration (d)	Precipitation (mm)	PDD ( $\text{d } ^{\circ}\text{C}$ )	Pond	Local catchment	Net	Total	Melt	Precipitation	Net $\Delta V$	Total $\Delta V$
C	2014	01-Mar-14	01-Mar-14	0	0	0	325	39100	0.25	0.25	0.0	0.0	81.3	81.3
C	2014	15-Mar-14	21-Apr-14	37	41.4	59.6	600	39100	1.85	2.21	1724.5	1618.7	1110.0	1326.0
D	2014	06-May-14	18-Jun-14	43	77.9	321.9	400	19400	1.10	2.65	4621.2	1511.3	440.0	1060.0
J	2013	11-May-13	11-Jun-13	31	76.6	237.1	7300	83800	1.22	1.79	14703.0	6419.1	8906.0	13067.0
J	2014	21-Apr-14	07-Jun-14	47	87.5	274.2	6000	83800	6.19	6.25	17003.7	7332.5	37140.0	37500.0
J	2013	9-Jun-13	9-Jun-13	0	–	–	7300	83800	0.18	–	–	–	1314.0	–
I	2014	31-May-14	31-May-14	0	0	7.4	900	29772	-0.01	0.04	163.0	0.0	-7.2	36.0
J	2014	22-May-14	28-May-14	6	37	33.3	6000	83800	0.06	0.23	2065.0	3100.6	360.0	1380.0
D	2014	22-May-14	28-May-14	6	37	33.3	500	19400	0.30	0.42	478.1	717.8	150.3	210.4
D	2014	02-Aug-14	02-Aug-14	0	–	–	500	19400	0.43	–	–	–	215.4	–
J	2014	21-Apr-14	21-Apr-14	0	–	–	4000	83800	1.09	–	–	–	4360.0	–

**Table S2.** Reference values relating to conduit incision for debris-covered glaciers. Values from Gulley et al. (2009) for conduit gradient are for Khumbu Glacier. Modelled spillway incision rates from Jarosch and Gudmundsson (2012) are the mean rate to conduit pinch-off in that study. Observed rates are water level lowering from the pressure transducer records. Estimated incision rates for the (Miles et al., 2016) discharge rate are determined by scaling the results of Jarosch and Gudmundsson (2012) according to the log-log relationship with discharge and the linear relationship with gradient.

Source	Gradient	Discharge ( $\text{m}^3 \text{s}^{-1}$ )	Incision Rate ( $\text{m d}^{-1}$ )	Note
Gulley et al. (2009)	2%-10%	–	–	Cut-and-closure, Khumbu Glacier
Gulley et al. (2009)	2%	–	–	Debris-filled crevasse trace, Khumbu Glacier
Gulley et al. (2009)	29%	–	–	Compressive hydrofracture, Khumbu Glacier
Jarosch and Gudmundsson (2012)	3%	0.1	0.026	Modelled
Jarosch and Gudmundsson (2012)	3%	1	0.097	Modelled
Jarosch and Gudmundsson (2012)	3%	10	0.420	Modelled
Jarosch and Gudmundsson (2012)	6%	1	0.220	Modelled
Jarosch and Gudmundsson (2012)	9%	1	0.333	Modelled
Miles et al. (2016)	–	0.028	–	Pond C, 2013; mean modelled
Observed, this study	–	–	~0.03	Slow lowering (D and I in 2014)
Observed, this study	–	–	~0.22	Fast lowering (C in 2014, J in 2013)
Estimate, this study	3%	0.03	0.012	Scaled relative to Jarosch and Gudmundsson (2012)
Estimate, this study	9%	0.03	0.036	Scaled relative to Jarosch and Gudmundsson (2012)
Estimate, this study	30%	0.03	0.120	Scaled relative to Jarosch and Gudmundsson (2012)

**Table S3.** Example calculations of discharge ( $Q$ ) through porous media for a hypothetical englacial conduit of blocked with debris. Columns show different configurations of cross-sectional area ( $A$ ), hydraulic conductivity ( $K$ ), and hydraulic gradient ( $\nabla P$ ).

$A$ $\text{m}^2$	$K$ $\text{m s}^{-1}$	$\nabla P$	$Q$ $\text{m}^3 \text{s}^{-1}$
0.25	0.03	-3%	0.000225
0.5	0.03	-3%	0.00045
1	0.03	-3%	0.0009
2	0.03	-3%	0.0018
4	0.03	-3%	0.0036
1	0.3	-3%	0.009
1	0.003	-3%	0.00009
1	0.0003	-3%	0.000009
1	0.03	-10%	0.003
1	0.03	-30%	0.009
1	0.03	-100%	0.03

**Table S4.** Back-of-the-envelope calculations of water level lowering rates and estimated subaqueous melt. The record for pond C is divided into sections of consistent slope. Pond area is estimated based on the orthoimages and water level change. The subaqueous melt area is the mean subaqueous ice-contact area required to account for the reduction in pond volume with a melt rate of  $0.029 \text{ m d}^{-1}$ , the mean rate calculated by (Miles et al., 2016). Cliff length corresponds to the distance of surface contact between the pond and bare-ice, and is measured from the orthoimages. Required depth is the mean ice cliff contact depth needed to produce the mean lowering.

Pond	Year	Start	End	Duration (days)	Head change (m)	Pond area ( $\text{m}^2$ )	Rate ( $\text{m d}^{-1}$ )	Pond volume change ( $\text{m}^3 \text{ d}^{-1}$ )	Subaqueous melt area ( $\text{m}^2$ )	Cliff length (m)	Required depth (m)
C	2013, early	24-May-14	19-Jun-14	26	-0.40	600	-0.0154	-9	122	60	2
C	2013, middle	19-Jun-14	06-Jul-14	17	-1.53	500	-0.0898	-45	910	60	15
C	2013, overall	24-May-14	07-Jul-14	44	-2.32	500	-0.0527	-26	207	60	3
J	2013	10-Jun-14	23-Jun-14	13	-2.80	7000	-0.2154	-1508	39992	260	154
C	2014, steep decline	21-Apr-14	01-May-14	10	-2.23	900	-0.2230	-201	6921	60	115
C	2014, shallow decline	01-May-14	01-Aug-14	92	-1.10	200	-0.0120	-2	9	60	0
D	2014	06-Aug-14	15-Oct-14	70	-2.25	400	-0.0321	-13	63	100	1
I	2014	08-May-14	18-Aug-14	102	-3.58	900	-0.0351	-32	107	70	2



**Figure S7.** Pond J in (a) May 2013, (b-c) October 2013, (d-e) May 2014, and (f-g) October 2014, highlighting the large seasonal fluctuations in pond size. Panel (a) shows the pond system from the southwest, and panels (c), (e), and (g) provide subsequent views of the western half of the system from the southwest. Panels (b), (d), and (f) provide views of the eastern half of the system from the northeast. Approximate photograph positions indicated on Figure 7.

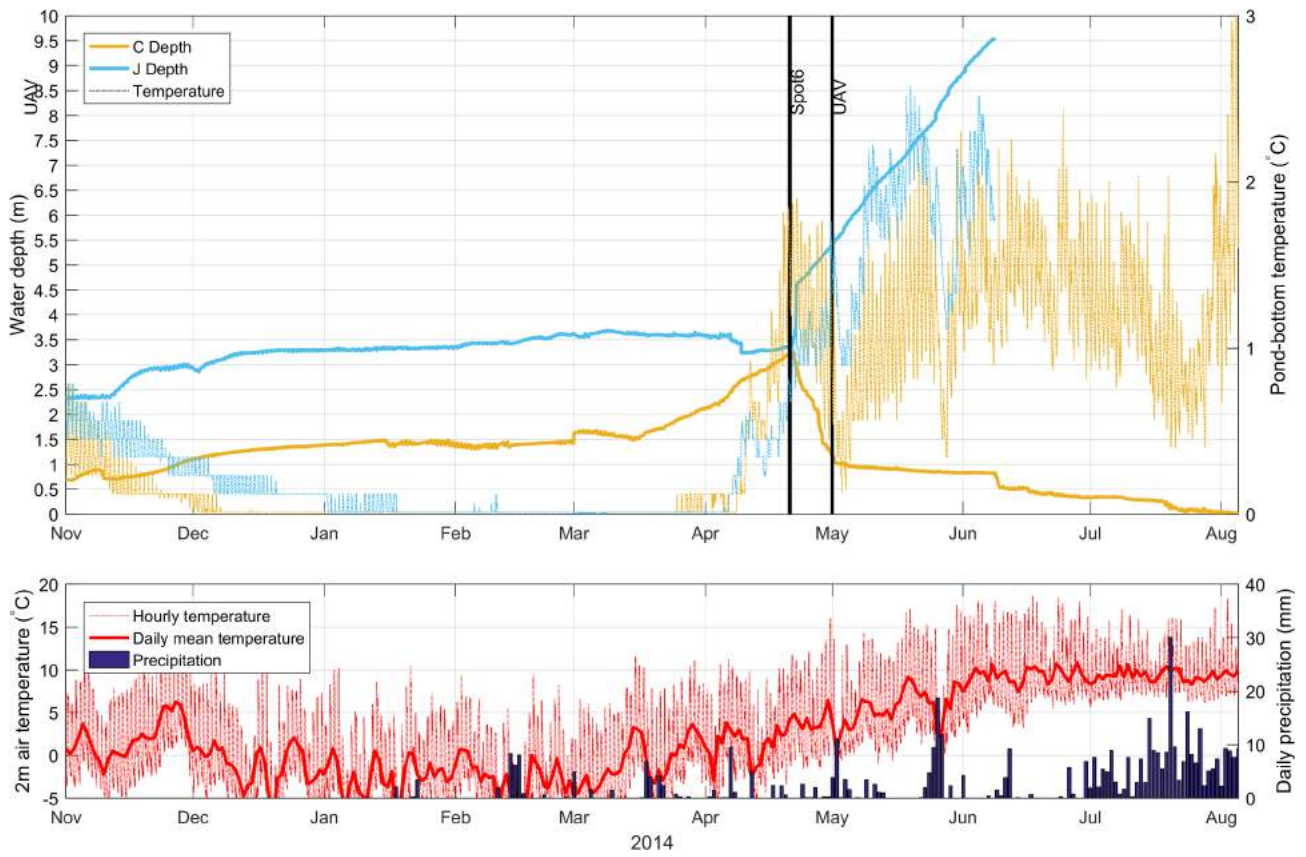


**Figure S8.** Records of pond C and J water level (relative to pressure transducer elevation) and temperature for the 2013-2014 winter. Also shown are air temperature from Lirung AWS and precipitation from Kyanjing AWS.



**Figure S9.** Crevasses evident during a field visit in October 2016 suggesting an extensional stress regime near the glacier headwall. This is a change from compressive crevasse traces observed in 2014 (Figure 1), and may be due to mass loading from a very large avalanche associated with the 2015 Gorkha earthquake (Ragettli et al., 2016).



**Figure S10.** Waterline melting led to the formation of thermo-erosional notches at many ponds during the study: (a) pond C in October 2013, (b) pond D in October 2014, (c) pond J in October 2013, and (d) a pond on Langtang Glacier in May 2013.